INL/JOU-20-58312-Revision-0

Irradiation Performance of Non-fertile (Pu-MA-Zr) Fast Reactor Metal Fuels

December 2020

Douglas L Porter, Luca Capriotti, Heather J MacLean Chichester, Pavel G Medvedev, Bruce A Hilton, Steven L Hayes

Changing the World's Energy Future

INL is a U.S. Department of Energy National Laboratory operated by Battelle Energy Alliance, LLC

INL/JOU-20-58312-Revision-0

Irradiation Performance of Non-fertile (Pu-MA-Zr) Fast Reactor Metal Fuels

Douglas L Porter, Luca Capriotti, Heather J MacLean Chichester, Pavel G Medvedev, Bruce A Hilton, Steven L Hayes

December 2020

Idaho National Laboratory
Idaho Falls, Idaho 83415

http://www.inl.gov

Prepared for the
U.S. Department of Energy
Under DOE Idaho Operations Office
Contract DE-AC07-05ID14517

Irradiation Performance of Nonfertile (Pu-MA-Zr) Fast Reactor Metal Fuels

H. J. M. Chichester, B. A. Hilton, S. L. Hayes, L. Capriotti*, P. G. Medvedev, and D. L. Porter*
Idaho National Laboratory
P. O. Box 1625, Idaho Falls, ID 83415-6188 U.S.A.

* Corresponding Authors Contact Information:

Luca Capriotti
Advance Characterization and Post-Irradiation Examination
Idaho National Laboratory
P.O. Box 1625
Idaho Falls, ID 83415-6188 U.S.A.
Phone: 1 (208) 533-7080
Email: Luca.Capriotti@inl.gov

Douglas L. Porter
Nuclear Science and Technology
Idaho National Laboratory
P.O. Box 1625
Idaho Falls, ID 83415-6188 U.S.A.
Phone: 1 (208) 533-7659
Fax: 1 (208) 533-7863
Email: Douglas.Porter@inl.gov

This manuscript has not been published elsewhere and has not been submitted simultaneously for publication elsewhere.

Abstract

This work was part of a program begun in 2001 to develop advanced nuclear fuels, originally as carriers for plutonium and minor actinides (neptunium, curium, and americium) taken from spent commercial light-water reactors (LWR) so that the plutonium and minor actinides could be 'burned' or transmuted in an accelerator or a fast nuclear reactor. A central part of these experiment programs has been the development of advanced fast reactor fuels, because a fast reactor was considered the most efficient vehicle to transmute the actinide waste products, and metallic fuels is a central focus of these tests. An experiment design was developed in which a thermal test reactor, the Advanced Test Reactor (ATR), was used to test small fuel pin prototypes, by creating areas in the core shielded by cadmium filters to produce a largely epithermal and fast neutron spectrum environment in which the pins could be irradiated. The results of non-fertile metallic fuel (no uranium) tests are presented here.

Pu-Am-Np-Zr fuels were irradiated to fission densities up to 33×10^{20} fission/cm^3 and Pu-239 depletions of up to 39%. The depletions were created by roughly 2/3 by fission and 1/3 by transmutation neutron capture. Up to five fuel 'rodlets' were irradiated in three sealed capsules stacked axially in the core, and the peak cladding temperatures ranged from 300°C to 500°C, depending on axial location as those near the core centerline are operating hotter and to higher fission densities. Several post-irradiation examinations (precision gamma scanning and fission gas release) were similar to other historical metal fuel experiments in fast reactors. However, optical metallography indicated that two of the rodlets had breached. The exact reasons are unclear. Due to the design of this irradiation experiment a rodlet breach could have increased the temperature in others in the same capsule by contaminating the thermal gap helium with heavier and less conductive fission product gases. Some of those rodlets showed high amounts of fuel/cladding chemical interaction (FCCI).

Keywords
fast reactor, metallic fuel, transmutation fuels, nonfertile, post-irradiation examination

Highlights
- Post-irradiation examination of nonfertile metallic fuels (no uranium) tests are presented here for a series of compositions with and without minor actinides.

- Precision gamma scanning and fission gas release results are similar to other historical metal fuel experiments in fast reactors.

1. Introduction

Since 2001, a program began to develop advanced nuclear fuels, originally as carriers for plutonium and minor actinides (neptunium, curium, and americium) taken from spent commercial light-water reactor (LWR) so that the plutonium and minor actinides could be 'burned' or transmuted in an accelerator or a fast nuclear reactor. Originally part of the Advanced Accelerator Applications (AAA) Program, the program's emphasis moved from accelerator technology to fast reactor technology and the program became part of Advanced Spent Fuel Treatment and Transmutation Research, which later became the Advanced Fuel Cycle Initiative, and then it became part of the Global Nuclear Energy Partnership, where the purpose and design of the fuels became more varied [1,2].

A central part of these experiment programs has been the development of advanced fast reactor fuels because a fast reactor was considered the most efficient vehicle to transmute the actinide waste products. Part of the concept development was to do an irradiation testing of the fuel types, which included metallic alloys, mixed oxides, and mixed nitrides. The emphasis was on metal fuels, which eventually dominated this program.

The testing part of the program was difficult because, unfortunately, the world now has few fast reactors capable of being used for fuel testing. As part of the AAA program, the Phénix reactor in Marcoule, France was one of the last available fast reactors and the U.S. and France began an experiment (the FUTURIX-FTA) [3,4] where Pu-Zr/U-Pu-Zr fuel, containing minor actinides and rare earth fission products, was irradiated. The experiment began irradiation in 2007 and has now been examined and reported [5]. A few other experiments akin to this were performed by other entities. Then it was proposed that a thermal test reactor could be used for limited testing [6].

An experiment design was developed in which a thermal test reactor, the Advanced Test Reactor (ATR), was used to test small fuel pin prototypes, by creating areas in the core shielded by cadmium filters to produce a largely epithermal and fast neutron spectrum environment in which the pins could be irradiated [7, 8]**.** It is the purpose of this article to report the results of these irradiations, as they pertain to the metal fuels and specifically to the classes of test metal alloys designed for several basic purposes. These purposes of all of the experiments included irradiation of nonfertile fuels or low-fertile fuels, both containing minor actinides. In some cases, rare earths were added in concentrations that may be expected to be carried over during spent fuel processing; the rare earths are known to be a potential detriment to long-term cladding integrity.

This work will discuss the results of the fast-reactor fuel experiments in which nonfertile metallic fuels were irradiated. Nonfertile fuels are those that will most efficiently 'burn' minor actinides that have been collected from spent LWR fuel; they will not breed additional plutonium as they do not contain any uranium. The metal fuel alloys contain Pu, Am, and Np, alloyed with Zr to maintain a high melting temperature and deter FCCI.

2. Experimental Details

Nonfertile fuels were tested with the intent to demonstrate the fuel performance of fast-reactor fuel containing no uranium (nonfertile), only plutonium and other minor actinides (neptunium and americium), which were to be a result of processing of spent LWR fuel [9]. Alloying elements, in this case zirconium, were added to increase the fuel melting temperature, phase stability, and resistance to fuel/cladding chemical interactions. The experiment was called AFC-1, in which capsules AFC-1B, AFC-1D contained five fuel rodlets each (AFC-1B and AFC-1D) of nonfertile metal fuel and AFC-1G contained two. AFC-1B was to be retrieved at a relatively low fuel burnup (4–8% of the initial Pu-239 content) and examined, while AFC-1D would achieve a much higher burnup (25–40% of the initial Pu-239 content) before being retrieved and examined.

The alloys were arc melted and cast to form a 3.8-cm fuel slug (sometimes in several segments) then sealed into and sodium bonded to HT-9 cladding, 0.584 cm in diameter. Figure 1 shows a sketch of the 'rodlet' as fabricated. Design parameters are shown in Table 1. Note that ~1.3 cm of sodium remains in the rodlet plenum to ensure that the fuel column is covered, while also filling the annulus between fuel and cladding.

Up to six rodlets were then stacked in a single outer capsule of Type 316 stainless steel (shown as well in Figure 1). The rodlets were thermally bonded to the outer capsule using helium gas, the gas gap between rodlet and capsule used to create the fuel and cladding temperatures of interest. The ATR is water-cooled and does not operate with coolant temperatures high enough to create the fuel and cladding temperatures representative of a typical fast reactor without the use of the gas gap.

The fuel alloy compositions (nominal) are also shown in Table 1 in weight percent. The amount of Zr alloy is very high 40–60 wt%, or 64–80 at.%. The lower melting temperature of the higher actinide alloys requires the additional alloying to ensure that the fuel alloy will not melt during expected upset conditions in the reactor [10].

The environment is somewhat different for these experiments, being irradiated in a reactor that generates a thermal neutron spectrum, even with Cd filters to partially harden the average neutron spectrum [7]. The neutron exposure to the materials, like the cladding, is lower than one would expect in a fast reactor (low fast fluence to fuel burnup [BU] ratio) and there is a small 'rim' effect in the fission rate because the neutron spectrum remains somewhat 'soft', dominated by epithermal neutrons.

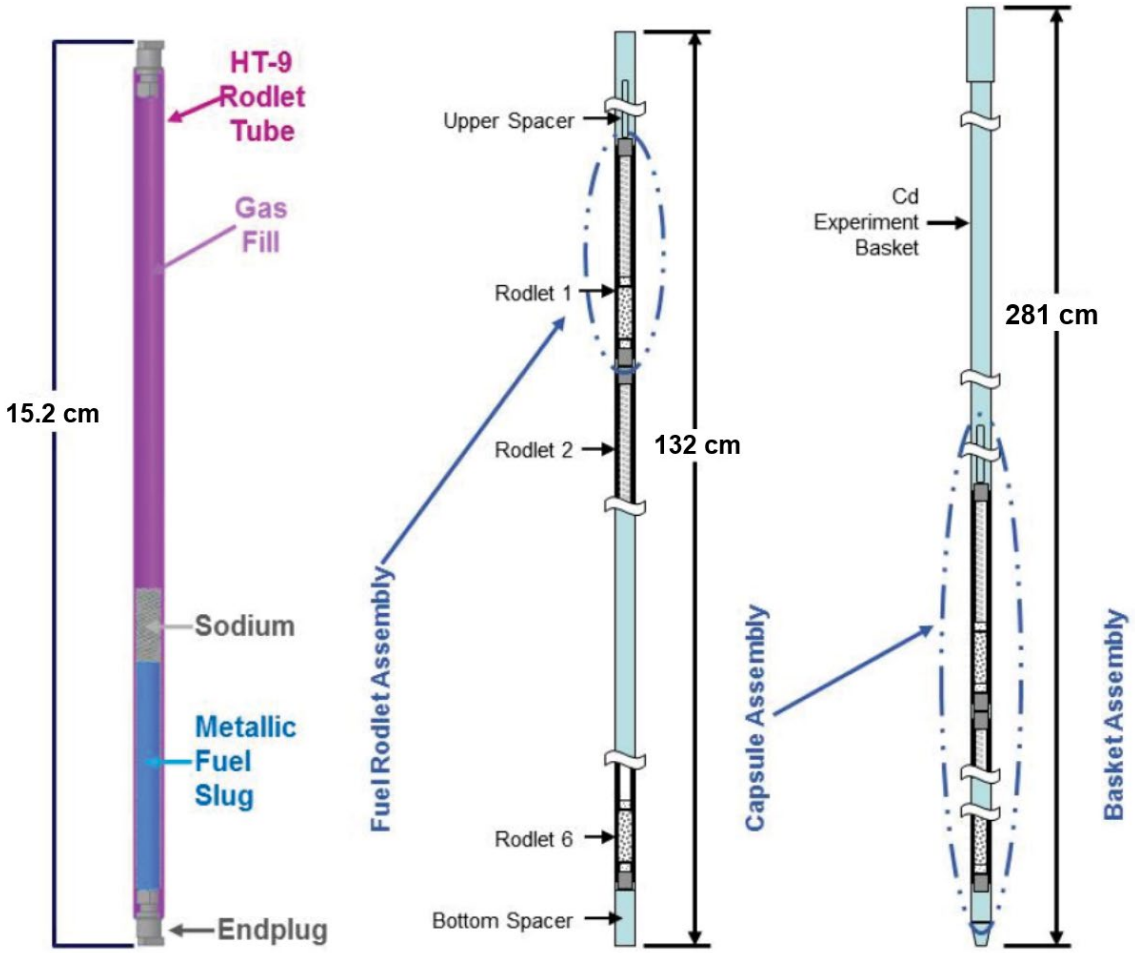

Figure 1. Sketch of a typical fuel rodlet,capsule and Cd-basket assembly used for the AFC-1B, 1D, and 1G experiments to test sodium-bonded nonfertile metal fuel in the Advanced Test Reactor.

Table 1 shows the design characteristics of the rodlets used in these tests. Note the variety of compositions.

Table 1. Design Characteristics of Experiment AFC-1B, -1D, and -1G.

Design Parameter	Design Value	As-Built
Cladding Material	HT9	HT9
Cladding OD, cm	0.584	0.584
Cladding ID, cm	0.49	0.49
Bond Material	sodium	sodium
Fuel Smeared Density	67%	60–63%
Fuel Alloys, wt%	Pu-40Zr Pu-60Zr Pu-10Np-40Zr Pu-12Am-40Zr Pu-10Am-10Np-40Zr	Pu-40Zr Pu-60Zr Pu-10Np-40Zr Pu-12Am-40Zr Pu-10Am-10Np-40Zr
Fuel Slug OD, cm	0.40	0.38–0.39
Fuel Height, cm	3.8	3.8–3.9(r5:2.5)*
Plenum Volume, cm^3	1.57	N/A

*The fuel height for rodlet 5 ('r5') of AFC-1B and AFC-1D is 2.5 cm

Note that the fuel smeared densities were all somewhat less than the design and length of the fuel column for rodlet 5 (R5, Pu-60Zr), both AFC-1B and 1D was also less than the design.

Experiments AFC-1B, AFC-1D, and AFC-1G contained five, five, and two nonfertile metal fuel rodlets, respectively, having the nominal and measured compositions shown in Tables 2, 3, and 4. Note that 1B and 1D contained the same fuel compositions. The Pu feed material for the experiments was ~82.8% Pu-239 for the fuel pins fabricated for these experiments.

Table 2. Nominal and measured compositions of rodlets AFC-1B.

Rodlet Number	1	2	3	4	5
Fuel Nominal Composition	Pu-12Am-40Zr	Pu-10Am-10Np-40Zr	Pu-40Zr	Pu-12Am-40Zr	Pu-60Zr
U (wt%)	0.00	0.00	0.00	0.00	0.00
Pu (wt%)	48.83	40.13	59.11	48.48	39.67
Am (wt%)	12.40	10.8	0.32	11.96	0.00
Np (wt%)	0.23	9.50	0.00	0.27	0.00
Zr (wt%)	41.00	41.00	41.00	40.80	60.70
N (wt%)	0.00	0.00	0.00	0.00	0.00
C (wt%)	NM	NM	0.008	NM	0.194
O (wt%)	NM	NM	0.069	NM	0.020
Na Mass (grams)	0.49	0.49	0.49	0.49	0.41

NM = not measured

Table 3. Nominal and measured compositions of rodlets AFC-1D.

Rodlet Number	1	2	3	4	5
Fuel Nominal Composition	Pu-12Am-40Zr	Pu-10Am-10Np-40Zr	Pu-40Zr	Pu-12Am-40Zr	Pu-60Zr
U (wt%)	0.00	0.00	0.00	0.00	0.00
Pu (wt%)	48.36	39.75	59.34	48.14	39.72
Am (wt%)	11.90	10.50	0.31	11.40	NM
Np (wt%)	0.25	10.10	0.00	0.28	NM
Zr (wt%)	40.00	38.90	39.00	42.20	59.60
Na Mass (grams)	0.49	0.49	0.49	0.48	0.41

NM = not measured

Table 4. Nominal and measured compositions of rodlets AFC-1G.

Rodlet Number	1	4
Fuel Nominal Composition	Pu-10Np-40Zr	Pu-10Np-40Zr
U (wt%)	0.00	0.00
Pu (wt%)	49.79	50.30
Am (wt%)	0.00	0.00
Np (wt%)	8.76	7.86
Zr (wt%)	40.40	41.60
Na Mass (grams)	0.49	0.48

Tables 5 and 6 show the final calculated fuel burnup (BU) attained by the rodlets in terms of percent burnup of Pu-239 (see Table 5) and fission density (expressed everywhere as f/cm^3) (see Table 6). The Pu-239 BU reflects the efficiency of 'burning out' the Pu, while the fission density better reflects the density of fission products, and the fission products create both fuel swelling and FCCI phenomena. Also, note that these experiments were done in the Cd-filtered spectrum of a thermal reactor, so the Pu-239 depletion results are not exactly what would be expected in a fast reactor.

The variation in BU (Pu-239 depletion) in Table 5 is created not only by residence time but also axial position (positions 3 and 4 are closest to the core axial center), fuel composition, and density. Note also that the Pu-239 depletion is caused by both fission and transmutation (neutron capture), with both types of events causing the disappearance of Pu-239. The ratio of these events for the Cd-shrouded fuel is about two fission events for every three Pu-239 atoms depleted [8]. It is therefore difficult to make an easy comparison between fission density and Pu depletion, even in the simple fuel composed of only Pu and Zr.

The fission density reflects the accumulation of fission products more accurately than the burnup of plutonium and therefore also reflects the fission-gas-generated fuel swelling and fission product effects on cladding. Table 7 shows the linear heat generation rate (LHGR, W/cm) as averaged over the cycles the rodlets were irradiated. Note that varying densities of Pu are depicted by the different fuels, such as lower concentration of Pu in

the Pu-60Zr fuel, in position 5, compared to the Pu-40Zrfuel, in position 3, has created a lower fission density than even the axial location would suggest if the fuels had the same composition. The Pu density in Pu-40Zr is 6.5 gPu/cm^3 and only 4.3 gPu/cm^3 in Pu-60Zr. If the Pu burning efficiency is accurately built into the fission density calculation, and the Pu densities are accurately known, then the depletions can be accurately calculated.

Peak cladding temperatures were calculated using the LHGR, which were calculated for each ATR cycle, and a thermal/hydraulic model developed using BISON [7]. These temperatures are plotted against the fission density, also calculated at these same intervals, in Figures 2–4. Note that the rodlets central to the fuel column (R3 and R4) have higher fission rates and therefore show higher fission densities.
. A simplified calculation of the Pu depletion can be done using equation (1).

$$D_{Pu\text{-}239} = [f_{dtotal} \bullet (f_{d239}/f_{dtotal})] / [(0.67) \bullet \rho_{Pu\text{-}239}] \qquad (1)$$

where, $D_{Pu\text{-}239}$ is the Pu-239 depletion; f_{dtotal}, the total fission density; f_{d239}, the fission density from Pu-239 fissions.

The calculation of the depletion of the various actinide species, such as Am, Np, and Pu, uing equation (1) was performed post-irradiation and checked with analytical chemistry methods [7, 8]. The calculated depletions are shown in Table 5. The results of this and a comparison with calculated values is shown subsequently in section 3.4 and table 9.

Table 5. Fuel Depletion (% Pu-239 depleted) for AFC-1B, -1D, and -1G Test Rodlets.

Rodlet	AFC-1B / AFC-1D †	AFC-1B Depletion (% of Pu-239)	AFC-1D Depletion (% of Pu-239)	AFC-1G Depletion (% of Pu-239)
1 (B/D)	Pu-12Am-40Zr	4.22	24.13	
2 (B/D)	Pu-10Am-10Np-40Zr	5.52	30.79	
3 (B/D)	Pu-40Zr	5.74	33.34	
4 (B/D)	Pu-12Am-40Zr	5.86	34.08	
5 (B/D)	Pu-60Zr	4.67	28.67	
1(G)	Pu-10Np-40Zr			24.49
4(G)	Pu-10Np-40Zr			33.20

† Alloy composition expressed in weight percent.

Table 6. Fission Density for AFC-1B, -1D, and -1G Test Rodlets.

Rodlet	AFC-1B / AFC-1D †	AFC-1B Fission Density 10^{20} f/cm^3	AFC-1D Fission Density 10^{20} f/cm^3	AFC-1G Fission Density 10^{20} f/cm^3
1	Pu-12Am-40Zr	2.9	19.6	
2	Pu-10Am-10Np-40Zr	3.4	22.4	
3	Pu-40Zr	5.3	33.0	
4	Pu-12Am-40Zr	4.3	28.4	
5	Pu-60Zr	3.5	22.5	
1(G)	Pu-10Np-40Zr			20.4
4(G)	Pu-10Np-40Zr			29.8

† Alloy composition expressed in weight percent.

Table 7. Linear Heat Generation Rate for AFC-1B, -1D and -1G Test Rodlets.

Rodlet	AFC-1B / AFC-1D †	AFC-1B Average LHGR (W/cm)	AFC-1D Average LHGR (W/cm)	AFC-1G Average LHGR (W/cm)
1	Pu-12Am-40Zr	128	134	
2	Pu-10Am-10Np-40Zr	149	153	
3	Pu-40Zr	223	228	
4	Pu-12Am-40Zr	184	194	
5	Pu-60Zr	150	151	
1(1G)	Pu-10Np-40Zr			131
4(1G)	Pu-10Np-40Zr			192

† Alloy composition expressed in weight percent.

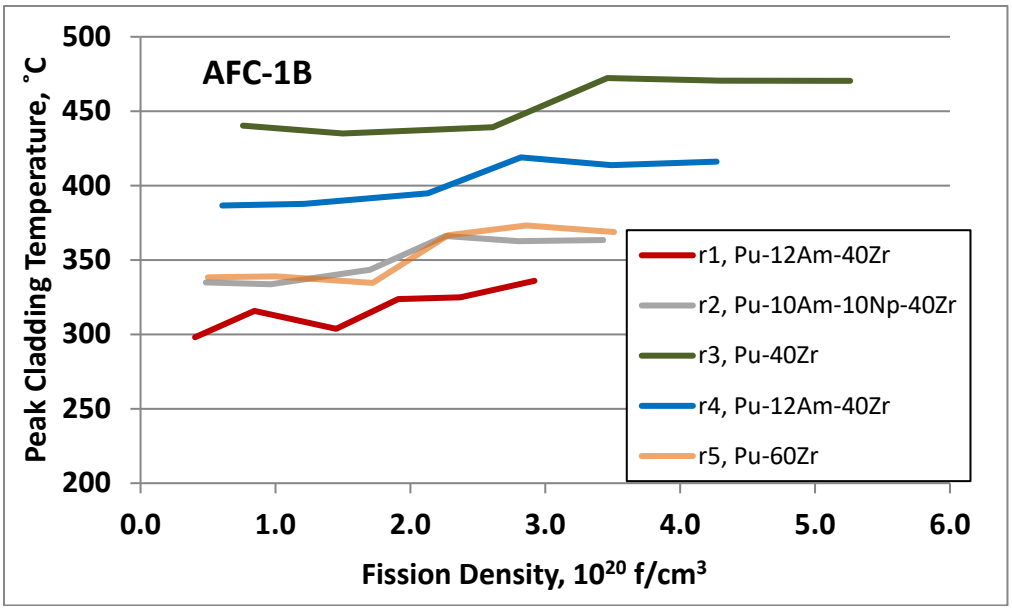

Figure 2. Peak cladding temperature for fuel rodlets in test AFC-1B. Values are adjusted for differences in the linear heat generation rate for each reactor cycle.

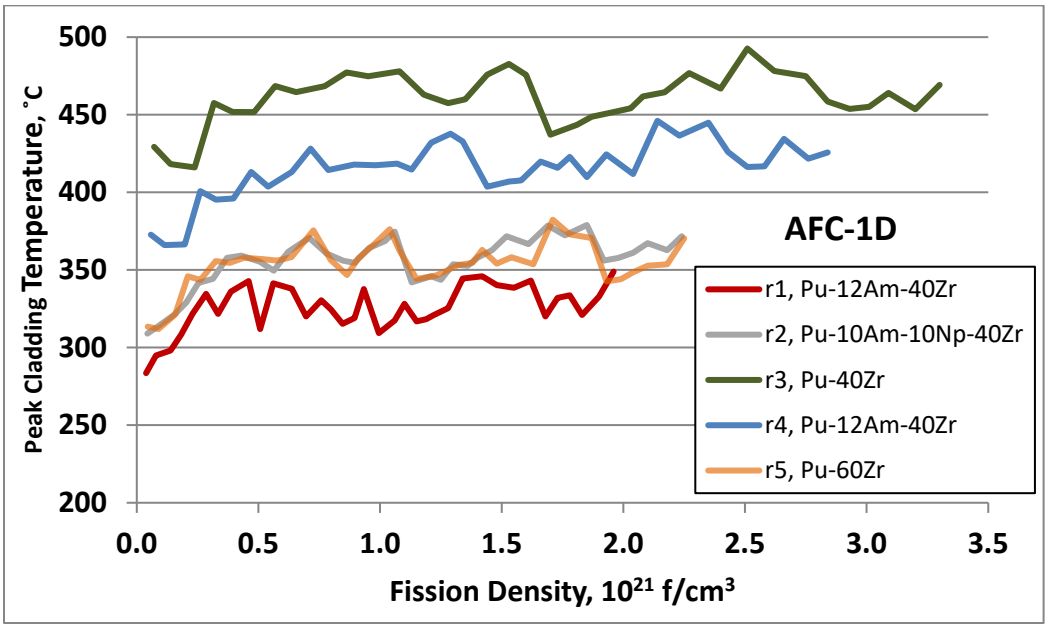

Figure 3. Peak cladding temperature for fuel rodlets in test AFC-1D. Values are adjusted for differences in the linear heat generation rate for each reactor cycle.

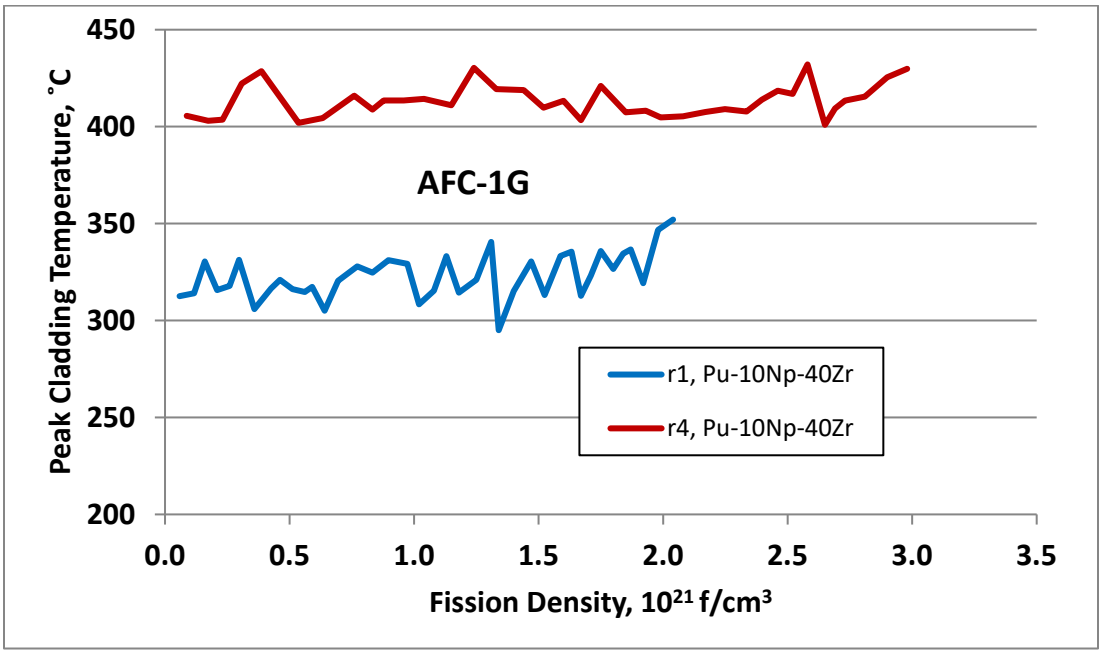

Figure 4. Peak cladding temperature for metal fuel rodlets in test AFC-1G. Values are adjusted for differences in the linear heat generation rate for each reactor cycle.

3. Post-Irradiation Examination

Following irradiation, the capsules AFC-1B,1D, and 1G were removed from reactor and transferred to the Hot Fuel Examination Facility (HFEF) at the Materials and Fuels Complex of INL. Each capsule held six 'rodlets', so the capsules were neutron radiographed to exactly locate the rodlets and help with further disassembly. The rodlets were then removed from the capsules for further examination. The examinations included a second neutron radiograph, precision gamma scanning, fuel cladding diameter axial profiling, and sampling of the plenum gas volume, pressure, and composition (atomic and isotopic). The rodlets were then sectioned for metallography, cladding hardness, and fuel burnup (chemical analysis for fission product concentrations).

3.1. Neutron Radiography and Precision Gamma Scanning

The rodlets were all radiographed using a neutron beam from a TRIGA reactor. Indium and dysprosium foils were placed behind the rodlets to be activated by the neutrons penetrating the rodlets, the indium foils being activated by epithermal neutrons and the dysprosium foils by thermal neutrons, respectively. The In and Dy foils were then used to activate radiation-activated film to show the image of the rodlets. By using the two types of images and brightness/contrast variations, the radiographs could be used to highlight features of the irradiated fuel slugs within the HT9 stainless-steel cladding and even the bond sodium above the fuel slug.

Precision gamma scanning was done to note the positions of mobile fission products, such as Cs-137 and Cs-134 isotopes and one of the many mobile rare earth fission products (in this case Pr-144). Mn-54 was used to note the position of the stainless-steel cladding and end plugs. Relatively immobile fission product species such as Ru-103 were also tracked. Other immobile species such as Nb-95 or Ru-106 were also found. Experience has shown that Cs often gets trapped in Na, either by reacting with Na logged in the fuel meat or combining with the sodium bond in the fuel pin plenum. The rare earths are expected to migrate to cooler regions of the fuel column. Combining gamma scan results with neutron radiography indicates at what fuel features the mobile fission products have accumulated.

Note that the precision gamma scanning of rodlets from AFC-1B were performed using a system that was aging, and the data for some isotopes proved to not be reliable. For example, the Ru-103 data often could not be used, so Nb-95 was substituted, representing the immobile fission product.

Figure 5 and Figure 6 show the gamma scanning information and simple thermal neutron produced radiographic image of the lower burnup/fission density AFC-1B (Figure 5) and higher burnup/fission density AFC-1D (Figure 6) HT-9 clad Pu-12Am-40Zr fuel. At the low fission density, the Cs has not redistributed to the plenum region of the rodlets, likely because the fuel swelling has not been great enough to allow for much interconnection of the pores. In the higher fission density AFC-1D Pu-12Am-10Zr rodlets, there are well defined Cs peaks in the bond sodium region above the fuel column. Note that the brightness/contrast in the top radiograph images in both Figure 6a and 6b were modified

to reveal how the sodium/fission product mixtures in the gas plenum of the rodlets are aligned with the top of the fuel column and axial positions corresponding to the location of Cs peaks. The stainless steel is also more activated, more clearly defining the position of the solid end plugs (see Mn-54 intensities).

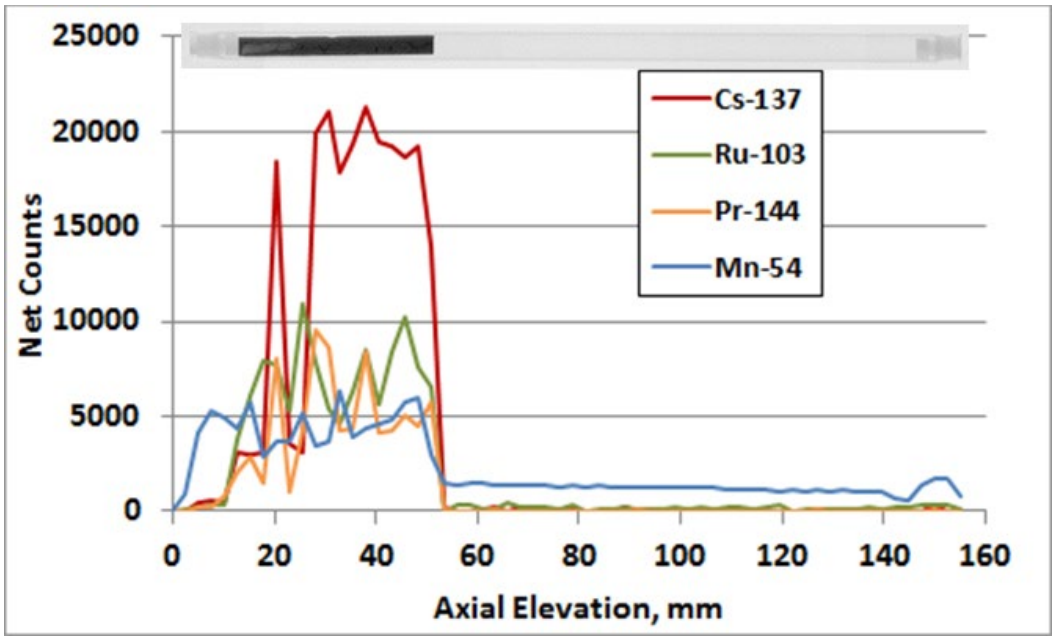

a) AFC-1B R1

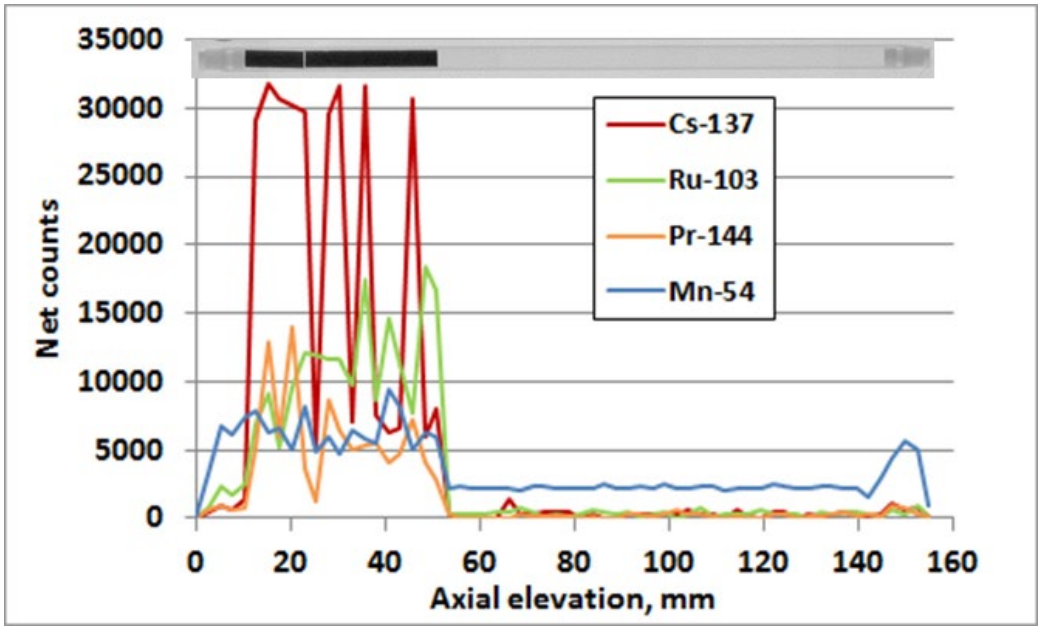

b) AFC-1B R4

Figure 5. Gamma scan analysis and neutron radiograph of Pu-12Am-40Zr from AFC-1B a) Rodlet 1 - 2.9 x 10^{20} f/cm^3 fission density and b) Rodlet 4 - 4.3 x 10^{20} f/cm^3 fission density.

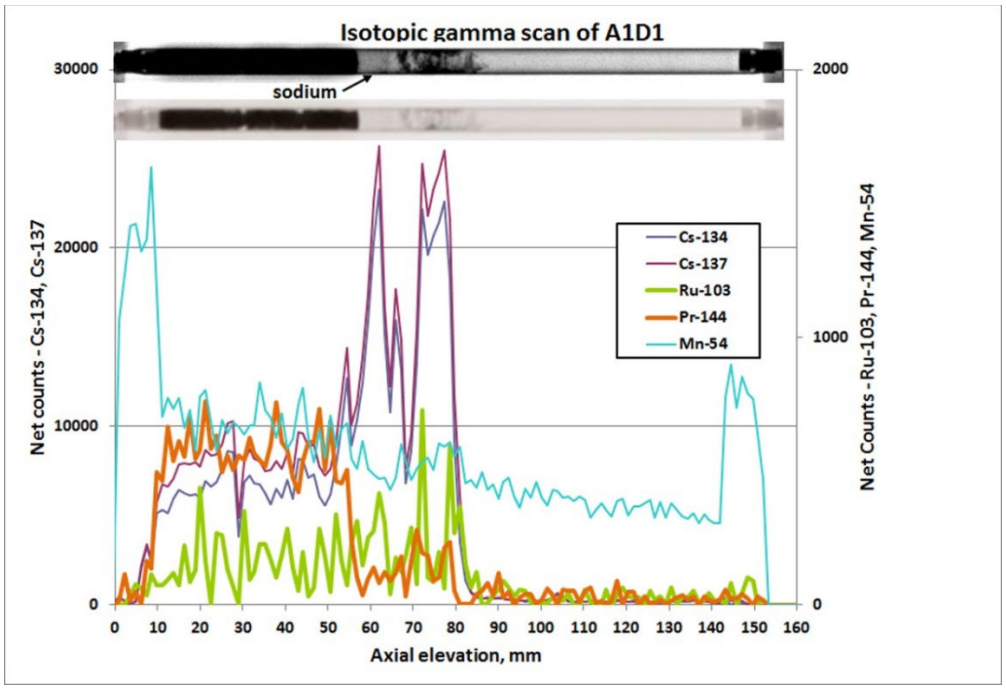

a) AFC-1D R1

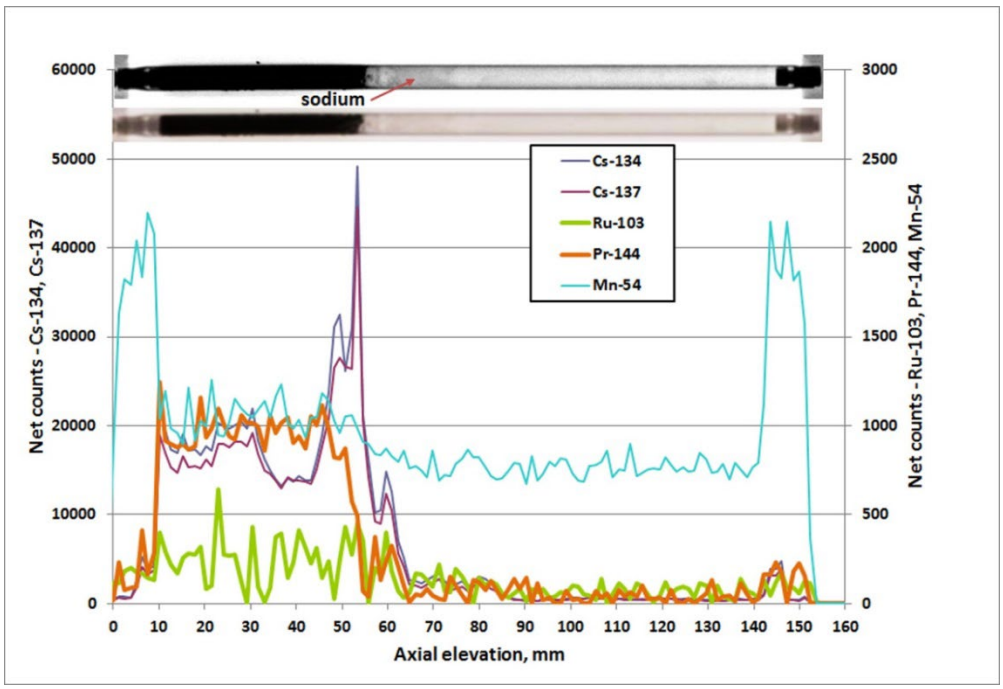

b) AFC-1D R4

Figure 6. Gamma scan analysis and neutron radiograph, with a duplicate enhanced to resolve bond sodium/Cs in the gas plenum, of the Pu-12Am-40Zr rodlets from a) AFC-1D Rodlet 1 - 19.6 x 10^{20} f/cm^3 fission density and b) Rodlet 4 - 28.4 x 10^{20} f/cm^3 fission density.

As mentioned previously, this behavior of Cs fission products has been observed many times before, Figure 7 showing one such example. The fuel represented in this figure was U-19Pu-10Zr clad with 316 stainless steel. Gamma scanning was performed on the same pins at a variety of fuel burnups, each pin being returned to the EBR-II reactor for further irradiation after an exam.

The Cs activity trace shows the same behavior as shown in Figures 5 and Figures 6 above. At low burnup (1.4 to 3.5 x 10^{20} f/cm^3) the Cs appears trapped in the fuel column, while at around 7.1 x 10^{20} f/cm^3 the fuel has swollen to the cladding, upon which the porosity links together and allows of fission gas and other mobile fission products to be released. The Cs accumulates in the bond sodium on top of the fuel column.

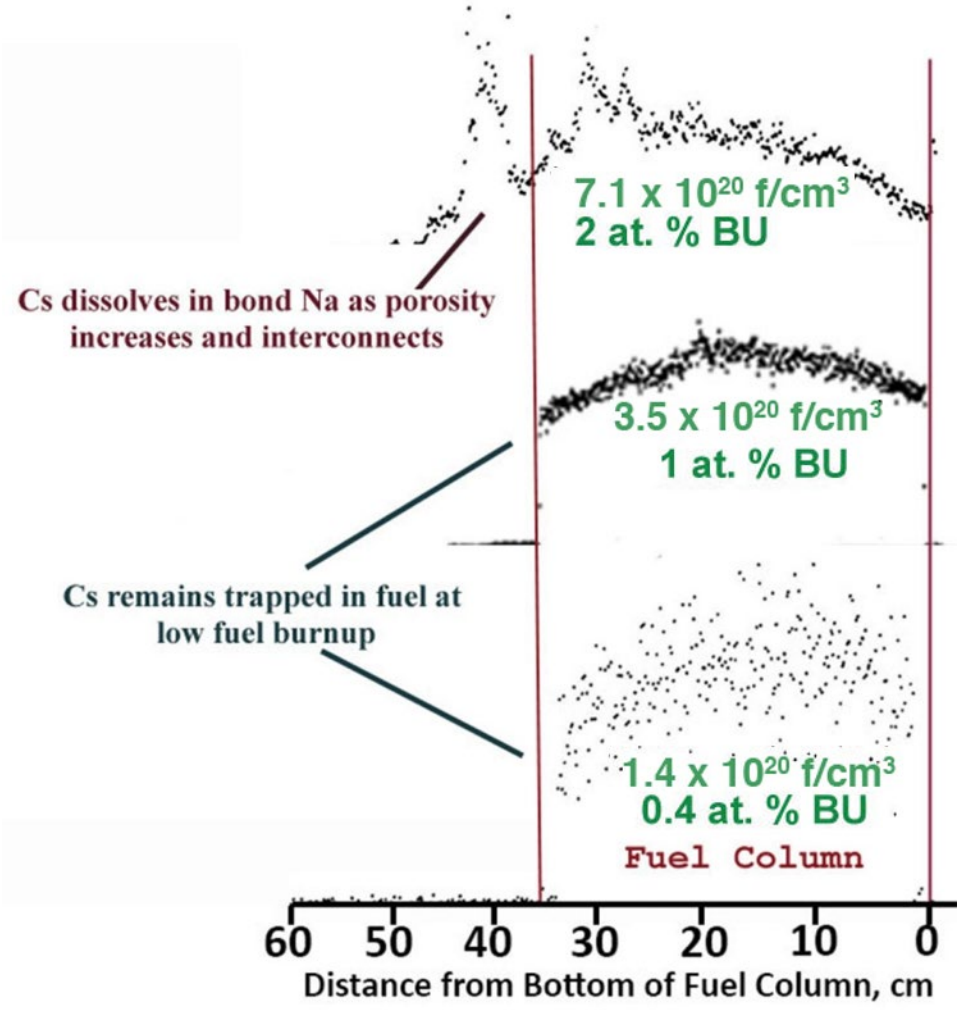

Figure 7. Cesium fission product release typical of fast reactor metallic fuels [11].

3.2. Metallography

Metallography was performed on axial cross-sections of the rodlets near the center of the fuel column. The images presented here (see Figure 8) are of as-polished surfaces. Note that many of the fuel columns still have small radii, except rodlet 3, the Pu-40Zr fuel with the highest fission density for this set (AFC-1B). Although it appeared to expand more, it also shows a large circumferential tear that could account for much of the radial growth.

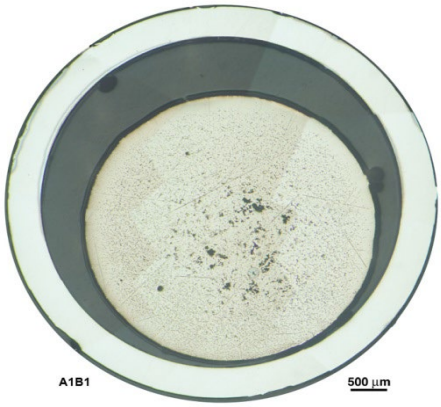

a) AFC-1B-R1

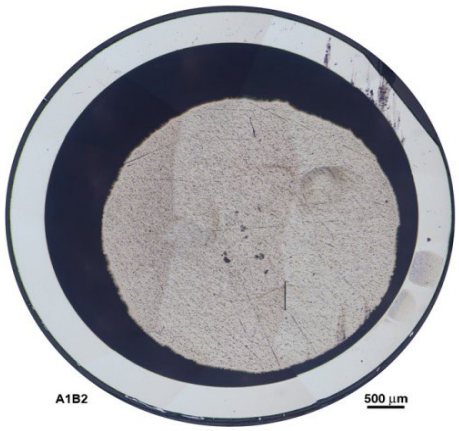

b) AFC-1B-R2

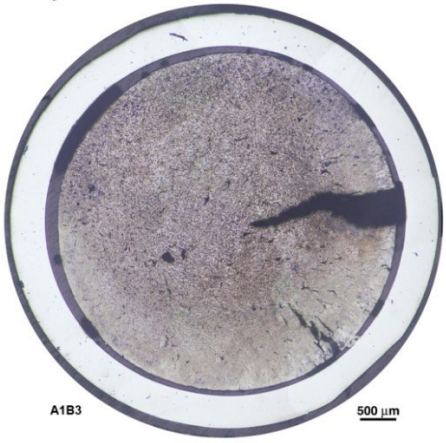

c) AFC-1B-R3

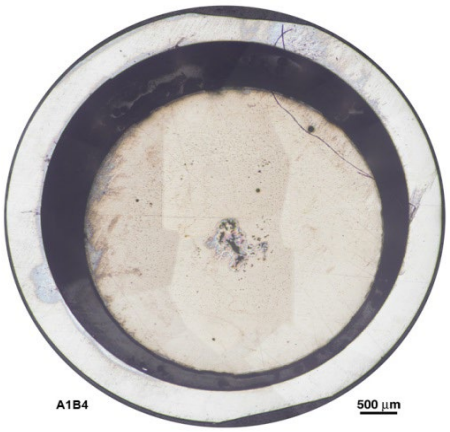

d) AFC-1B-R4

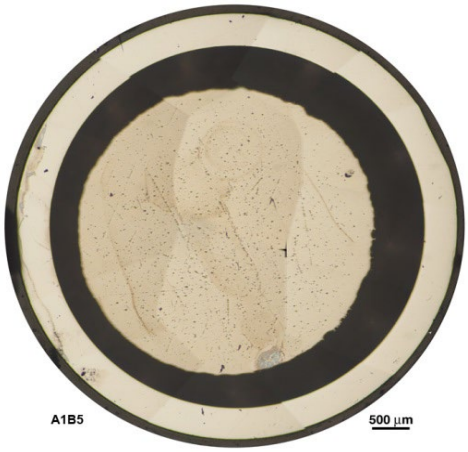

e) AFC-1B-R5

Figure 8. Cross-sectional metallography of AFC-1B metallic nonfertile samples as-polished a) 1B-R1-Pu-12Am-40Zr irradiated to 2.9 × 10^{20} f/cm^3, b) 1B-R2-Pu-10Am-10Np-40Zr irradiated to 3.4 × 10^{20} f/cm^3, c) 1B-R3-Pu-40Zr irradiated to 5.3 × 10^{20} f/cm^3, d) 1B-R4-Pu-12Am-40Zr irradiated to 4.3 × 10^{20} f/cm^3 and e) 1B-R5-Pu-60Zr irradiated to 3.5 × 10^{20} f/cm^3.

The set of these same fuel compositions irradiated to much higher fission density as AFC-1B, the AFC-1D fuels, were swollen radially to the cladding. The metallography (see Figure 9), however, was difficult as the outer radial regions of the fuel crumbled during preparation. Also, two of the fuel columns had breached during irradiation, as will be shown later when discussing the fission gas release results.

Assuming one of these rodlets failed during the irradiation cycles, the others may have overheated due to the mutual containment of the rodlets in a single capsule. If one of the five rodlets breached, it would have released fission gas into the gas plenum of the capsule. The majority of the fission gas is xenon. This failure mode has also been observed and reported for the AFC-2 series [12]. Of course, a breach caused by handling post-irradiation would negate this effect/conjecture.

Rodlet AFC-1D-R3 (see Figure 9c) shows a large amount of FCCI, as evidenced by the extra phases at the fuel cladding interface and the area where it appears that cladding is missing. The extra phases are likely comprised of fuel and cladding components.

There is an obvious crack in the cladding revealed in the AFC-1D-R4 mount (see Figure 9d). If created by simply overheating the cladding and adding internal pressure, the HT9 cladding would likely show a bulge in the cladding where the crack occurred. If influenced by other components, we would expect an area of embrittlement or a crack exhibiting the features shown.

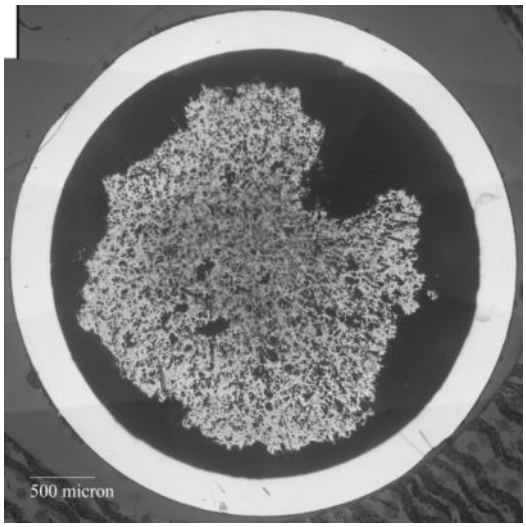

a) AFC-1D-R1

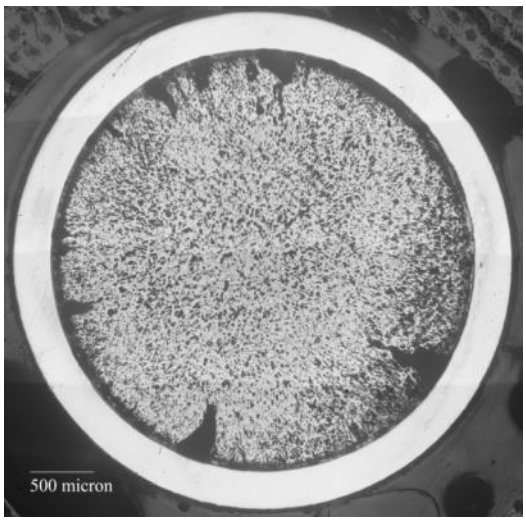

b) AFC-1D-R2

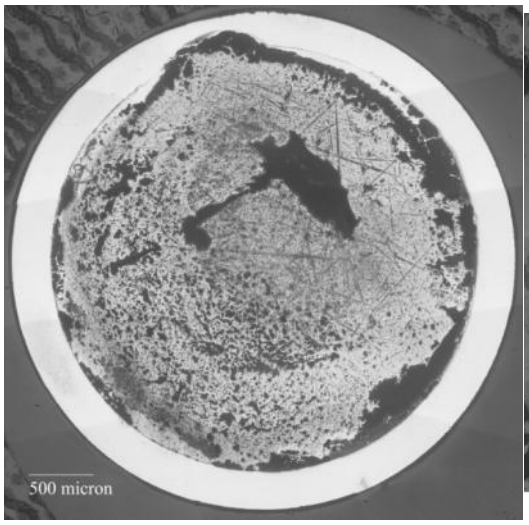

b) AFC-1D-R3 FCCI

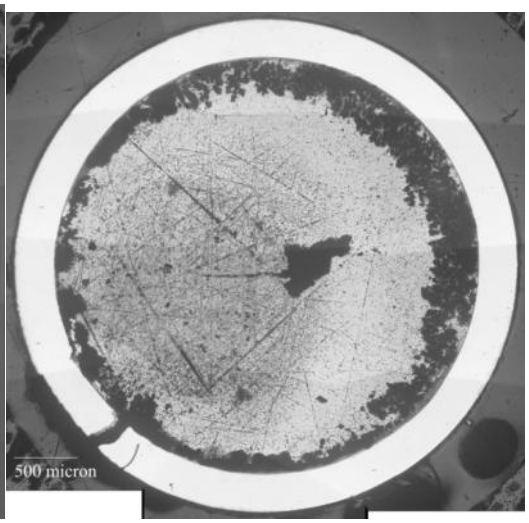

d) AFC-1D-R4 - breached

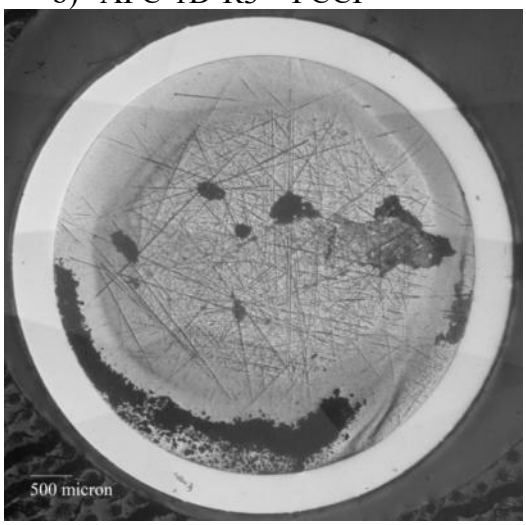

e) AFC-1D-R5

Figure 9. Cross-sectional metallography of AFC-1D metallic nonfertile samples as-polished a) AFC-1D Rodlet 1 irradiated to 19.6 × 10^{20} f/cm^3, b) AFC-1D Rodlet 2 irradiated to 22.4 × 10^{20} f/cm^3, c) AFC-1D Rodlet 3 irradiated to 33 × 10^{20} f/cm^3, d) AFC-1D Rodlet 4 irradiated to 28.4 × 10^{20} f/cm^3 and e) AFC-1D Rodlet 5 irradiated to 22.5 × 10^{20} f/cm^3.

As explained later in this manuscript, there was evidence that both AFC-1D-R3 and AFC-1D-R4 had breached during irradiation as well as the obvious crack in one (R4) and FCCI in the other (R3). The lack of plenum gas will be discussed in more detail after that data has been introduced, but in Figure 9 we see in the metallography that these two rodlets both had some rather extensive FCCI. Metallography was repeated to look more closely at that FCCI.

The metallography of AFC-1D, the higher burnup fuel, did not show the typical three-zone structure of fast-reactor tests of U-Pu-Zr fuel. This is not unexpected, as the phase fields represented for U-Pu-Zr were not the same for these fuels containing no uranium.

The phase diagram for Pu-Zr is not well understood at this high concentration of Zr as reported in [13], and there might be differences in elements/phases redistribution behavior among the different alloy compositions if consider for example Pu-40Zr (AFC-1D R3) compare with Pu-60Zr (AFC-1D R5) taking in consideration the presence or not of a miscibility gap at higher Zr content (~ 80at% Zr)

Figure 10 shows the re-polished section of AFC-1D-R3 as well as several higher magnification images of the FCCI (inset A and B taken from two different positions). The high-magnification inset B clearly shows different layers (indicated in the image as #1, #2, #3) in the FCCI structure near the fuel/cladding interface; inset A only clearly shows one (indicated in the image as layer #2).

The only literature reporting on fuel performance of U-free metallic fuel is in ref [5] in which the different phases and microstructure are associated with the available Pu-Zr phase diagram and compared with U-Zr / U-Pu-Zr behavior. No FCCI discussion is present in ref [5]. Therefore, taking in consideration that U and Pu in a U-Zr/U-Pu-Zr system are not the primarily contributors to FCCI and behave somehow similar interacting with the cladding, it is believed that for the sake of this FCCI discussion, the available literature on U-Zr and U-Pu-Zr is adequate.

Keiser [14] had previously discussed in detail the nature of most of these FCCI layers, formed when fuel and fission products (rare earths) interdiffuse with the cladding. Most recently, another metallic fuel sample U-10Zr clad in HT9 was examined, showing further insights into the FCCI layers [15].

The layers seen in Figure 10 were all described in the latter reference, but here, in the two rodlets that breached, there is evidence that at least one of the layers reached a melting temperature, unlike what was observed in the Harp study [15]. Note that there are bubbles in layer #3 in inset B and even some close to the fuel in the layer shown in inset A (layer #2).

Layer #1 is one that is often missed when examining the FCCI in HT9 clad metallic fuel. The large grain, showing no fine structure as would appear in martensitic steels, indicated that carbon loss has resulted in a martensite-to-ferrite conversion. The Harp study further showed, using SEM analysis, that rare earth (RE) fission products may also have infiltrated the cladding along these grain boundaries. Further study would be required to confirm this in AFC-1D-R3.
Furthermore, taking in consideration FCCI literature [14, 15] and the similarity in layer morphology, layer #2 is inferred to be largely RE fission products and cladding and it is visible in both inset A and B. Layer #3 might include also fuel constituents in large amounts, along with fission products and cladding components. Evidence of melting / incipient melting, especially in the area where the cladding is nearly penetrated, is visible.

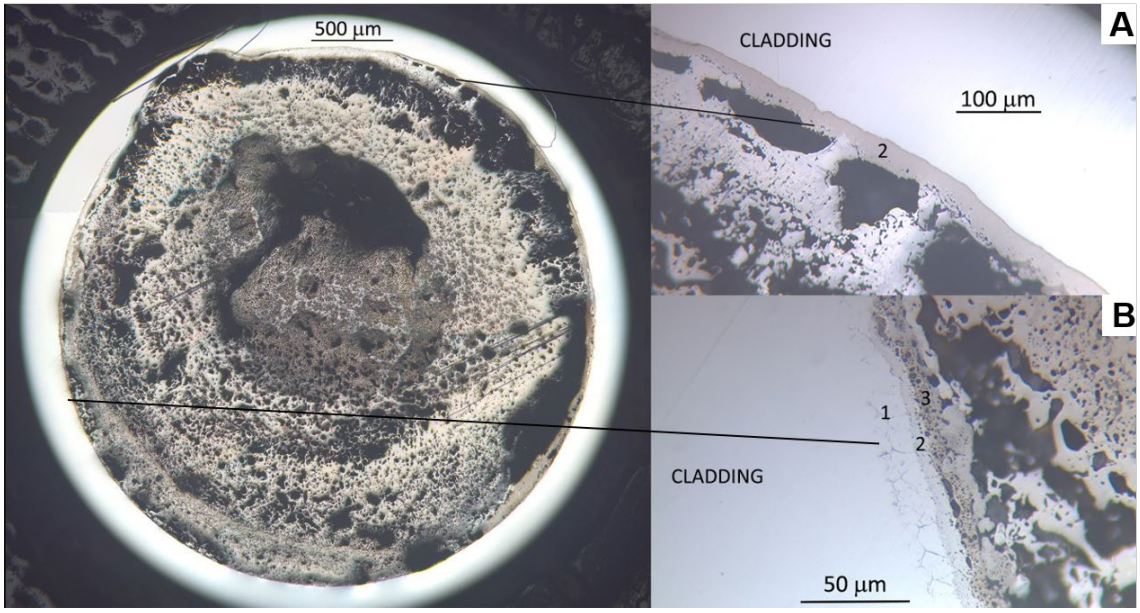

Figure 10. Re-polish of the transverse section of AFC-1D-R3 (left). The other two are higher magnification images (inset A and B, right) showing the three FCCI layers at the fuel/cladding interface.

Figure 11 shows a high-magnification optical microscopy image of the AFC-1D-R4 fuel/cladding interface. Again, the FCCI layers are shown, but the decarburized layer is not evident in the cladding. It may not be visible because the grain boundaries are not highlighted. Melting may also be indicated, but there are no large-scale areas as were evident in R3 (see Figure 10).

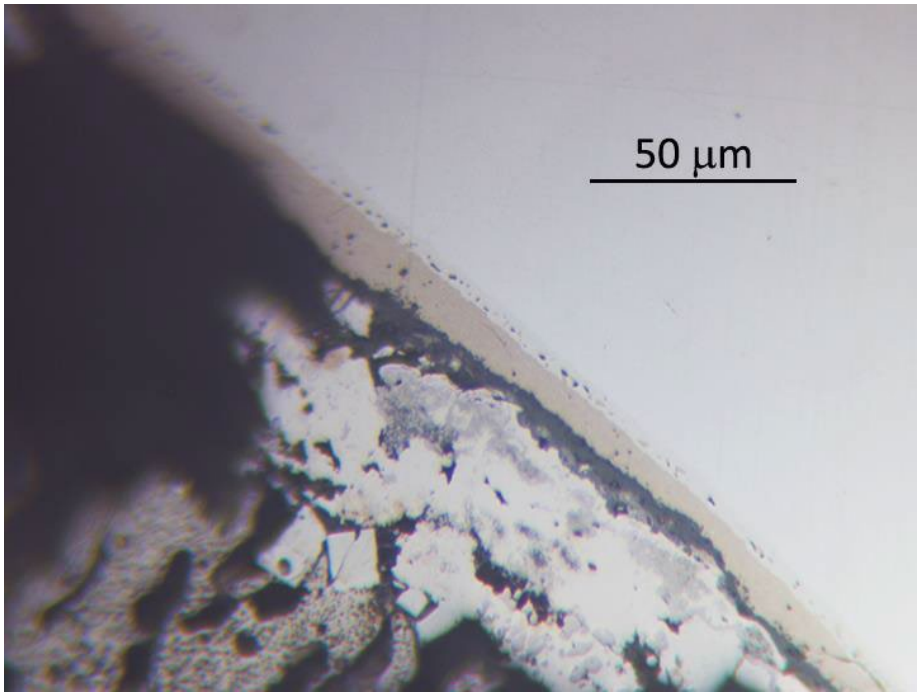

Figure 11. Metallographic image of the re-polished section of AFC-1D-R4 showing the FCCI at the fuel/cladding interface. Much the same layers are visible here as in Figure 10.

Finally, the last two metallography shown in Figure 12 are from AFC-1G-R1 and -R4, higher burnup comparable with AFC-1D fission density. The fuel has fully swollen in contact with the cladding in both samples but without apparent FCCI. Some changing in the microstructure aspect, perhaps correlated with preliminary redistribution of elements, is visible in the central part of the AFC-1G-R4 fuel sample.

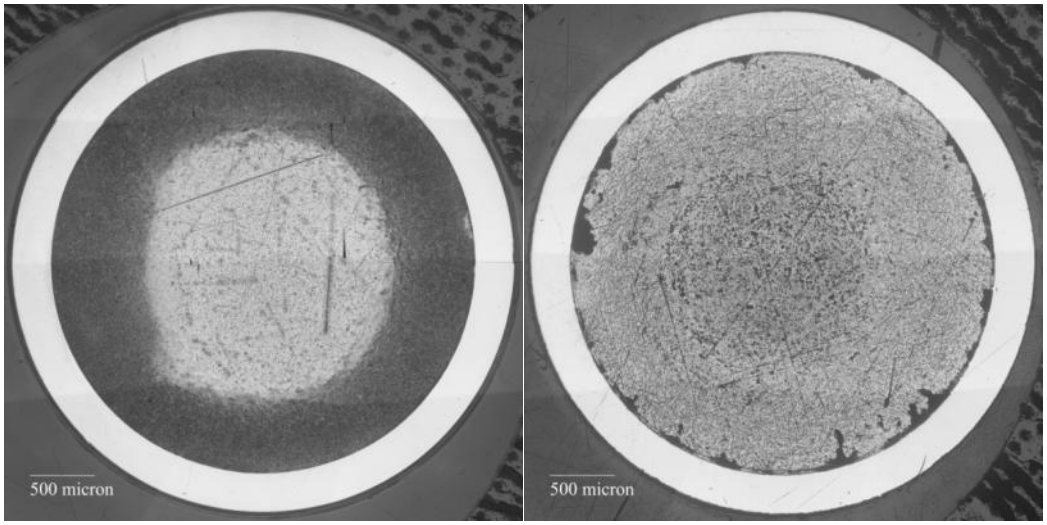

a) AFC-1G-R1 b) AFC-1G-R4

Figure 12. Cross-sectional metallography of AFC-1G metallic nonfertile samples as-polished a) AFC-1G-R1 irradiated to 20.4 × 10^{20} f/cm^3 (24.49 at.% depletion) and b) AFC-1G-R4, irradiated to 29.8 × 10^{20} f/cm^3 (33.20at.% depletion). Depletion in units of at.% Pu-239.

3.3. Fission Gas Release

Fission gas release, or retention in the fuel, is an important phenomenon in the performance of fast-reactor metal fuel. In modern fuel pin designs, the smeared density is low enough (75% or less) to allow the interconnection of fission gas pores as the cylindrical fuel column swells radially to contact the cladding. This allows a large fraction of the fission gas trapped in the fuel to be released into the plenum volume of the pin. If the gas were not released, the swelling fuel could exert enough force on the cladding to cause the cladding to creep and perhaps rupture. For this reason, the fission gas release characteristics of a fuel type is important in understanding its performance.

The amount of fission gas in the gas plenum of each rodlet was measured using the Gas Assay, Sample, and Recharge (GASR) system in the HFEF hot cell. The system utilizes a powerful laser to puncture a hole through the stainless-steel cladding into the gas plenum of a fuel pin/rodlet. The tube through which the laser light travels is sealed to the cladding so the system can trap any gases released from the plenum volume.

With a series of known volumes, the plenum gas is expanded into the GASR system. Then, measuring the pressure of the gas expanded into these volumes and using the ideal gas law, the pressure (P) and therefore the number of moles of gas, n, are calculated. Then, using known pressures/volumes of backfill gas, these amounts of gas are expanded into the empty gas plenum which has been evacuated. A series of these back-fills results in a measurement of the gas plenum volume. The GASR measurements are also used to confirm if a fuel pin/rodlet has sustained cladding breach.

A sample of the extracted gas from the original puncture of the gas plenum is analyzed using gas mass spectrometry. Xenon and krypton isotopes as well as a number of atomic gas species (xenon, krypton, oxygen, nitrogen, ethane, methane, argon, helium, carbon dioxide, C_xH_y, and tritium) are measured to determine the amount of xenon, krypton and helium that has been produced in the fuel and subsequently released into the gas plenum.

The amount of fission gas produced in a rodlet can be calculated using the fission density, fission yields, and isotope decay. Taking in consideration the as-built elemental gas composition, calculating the amount of fission gas, or helium, produced in a rodlet, and measuring the gas released to the plenum, the percentage of gas released is determined. Helium calculated generation was estimated to come only from americium transmutation.

The release fractions/percentages are shown in Table 8.

The pressures from fission gas (Xe and Kr) or He are very low for the AFC-1B rodlets, as expected; the fuel had not swelled much, so not much gas could be released by the interconnection of bubbles. Furthermore, the fission densities were low. The pin that showed the largest degree of swelling (including a circumferential tear), AFC-1B-R3, also showed the only measurable fission gas released among the low burnup AFC-1B rodlets.

Note that the pressures measured on puncturing for rodlets AFC-1D-R3 and -R4 were either ambient (hot-cell pressure) or somewhat low, although so was AFC-1G-R4. The gas sampling from both of these AFC-1D rodlets indicated that there was no Xe or Kr, only the Ar hot-cell atmosphere. However, for AFC-1G-R4, gas sampling was able to measure a Xe and Kr release, although the results seems spurious.

The remaining high burnup rodlets from AFC-1D and -1G present a Xe and Kr gas release as well as a He release that is in line with the historical trend of data collected for the U-Pu-Zr fast-reactor fuel pin [16] and also with the more recent data on other minor actinides nonfertile/fertile metallic fuel experiments [5].

Table 8. Fission Gas (Xe, Kr) and He Release from the Fuel to the Rodlet Gas Plenum.

Capsule	Rodlet	Plenum Pressure* (Pa)	Plenum Volume (cm^3)	Kr+Xe Gas Release (%)	He Gas Release (%)
1B	1	0.00/00.00	1.620	0	0
1B	2	69/139	1.628	0	0
1B	3	$5.7x10^4$/1800	1.625	26.5	17
1B	4	207/207	1.634	0	0
1B	5	69/0.00	1.867	0	0
1D	1	$2.06x10^6$	1.040	87.7	71.3
1D	2	$2.49x10^6$	0.975	89.1	74.0
1D	3	$1.04x10^5$	1.275		
1D	4	breached			
1D	5	$5.65x10^5$	1.222	75.1	98.6
1G	1	$8.6x10^5$	0.870	63.1	68.5
1G	4	$1.53x10^5$	0.955	>100	88.9

*from fission gases (FPs/He) where applicable; note that 1×10^5 Pa= 14.5 psi

3.4. Fission Product Chemistry – Burnup Analysis/Actinide Depletion

Chemical/isotopic analysis using Inductively Coupled Plasma-Mass Spectrometry (ICP-MS) was used to measure fission product concentrations as well as primary components. Table 9 and Figure 13 show the calculated and measured depletion values for Pu-239, Am-241, and Np-237, respectively. The high burnup AFC-1D and AFC-1G rodlets are both included as representative of these measurements.

Plutonium depletion numbers correlated best; the ratio is closest to 1.0. The data set is not large, but, if the correlation holds true, the low scattering of the Pu-239 depletion ratio could be caused by a better knowledge of the neutron capture (less error in the calculated depletion) and/or because there is a greater abundance of Pu-239 than the other species, making for perhaps a smaller inherent error in the measured values.

The good correlation between measured and calculated Pu depletion for most of the rodlets indicates the same depletion, or Pu burning efficiency, for the differing neutron spectra at most axial positions in the core. Positions 1 and 5 are furthest from the core and they are the exception. The depletion was a little lower in positions 1 and 5, supported by the close match of calculated and measured Pu depletions.

Table 9. Calculated and Measured Depletion Values for Pu-239, Am-241, and Np-237 for Rodlets AFC-1D and AFC-1G.

Fuel Rodlet	Composition, wt%	Calculated Depletion, at.%			Measured Depletion, at.%		
		Pu-239	Am-241	Np-237	Pu-239	Am-241	Np-237
AFC-1D r1	Pu-12Am-40Zr	24	45		26	39	
AFC-1D r2	Pu-10Am-10Np-40Zr	31	56	41	32	52	32
AFC-1D r3	Pu-40Zr	33			35		
AFC-1D r4	Pu-12Am-40Zr	34	60		39	52	
AFC-1D r5	Pu-60Zr	29			28		
AFC-1G r1	Pu-10Np-40Zr	25		33	21		28
AFC-1G r4	Pu-10Np-40Zr	33		46	30		38

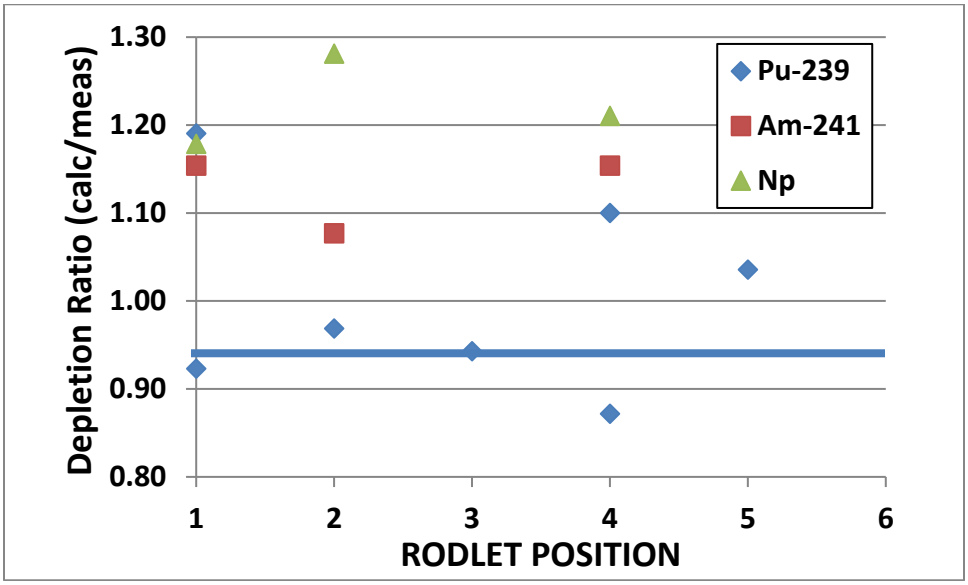

Figure 13. Ratio of calculated to measured depletion for Pu-239, Am-241, and Np-237 as a function of rodlet position. Rodlet positions 3 & 4 are near core center.

4. Conclusions

1. Pu-60Zr, Pu-12Am-40Zr, Pu-10Np-40Zr, and Pu-10Am-10Np-40Zr alloy fuel rodlets were irradiated in ATR with linear heat generation rates from 128 W/cm to 228 W/cm, creating peak cladding temperatures from 300 to 500°C (calculated). Metallography and gas release data indicated that two rodlets breached. One breach could have caused the other four in the capsule to also operate hotter, as the gas gap would have been contaminated with fission gases with lower thermal conductivities. Metallography did reveal higher than expected FCCI in one of the two breached rodlets.

2. Metallography of the fuels with high fission densities, in the AFC-1D and AFC-1G capsules, revealed no radial zone structure typical of Zr and U migration in fast-reactor tests of the U-Pu-Zr fuels. Without U present, the phase fields are different, so this was not unexpected.

3. Precision gamma scanning and gas release appeared to be similar to fast reactor tests of U-Pu-Zr fuel, showing the same behavior of migrating fission products, such as Cs-137.

4. Calculations of Pu-239 depletion matched reasonably well with post-irradiation chemical/isotopic analysis. The calculations were based on about 2/3 of the Pu-239 depletion created through fission and the other 1/3 through transmutation (neutron capture).

Disclosure Statement

Acknowledgements

The authors would like to thank Dr. Samuel Bays for the HELIOS calculations showing the Pu-239 and other actinide fission/transmutation splits in these experiments.
This work was supported by the U.S. Department of Energy, Advanced Fuels Campaign of the Nuclear Technology Research and Development program in the Office of Nuclear Energy.

Data Availability Statement

The raw/processed data required to reproduce these findings cannot be shared at this time due to technical or time limitations.

References

1. S.L. HAYES, B.A. HILTON, M.K. MEYER, G.S. CHANG, F.W. INGRAM, S. PILLON, N. SCHMIDT, L. LECONTE, D. HAAS, "**U.S. Test Plans for Actinide Transmutation Fuel Development**", in: Trans. Am. Nucl. Soc. Vol. 87, 2002: p. 353.

2. Report to Congress on the Advanced Fuel Cycle Initiative: **The Future Path for Advanced Spent Fuel Treatment and Transmutation Research** (2003).

3. L. DONNET, F. JORION, N. DRIN, S. L. HAYES, J. R. KENNEDY, K. PASAMEHMETOGLU, S. L. VOIT, D. HAAS and A. FERNANDEZ, "**The FUTURIX-FTA Experiment in PHENIX: Status of fuel fabrication,"** Proc. of GLOBAL 2005, Tsukuba, Japan, Oct 9-13, 2005 (Paper No. 258)

4. P. JAECKI, S. PILLON, D. WARIN, S.L. HAYES, J.R. KENNEDY, K. PASAMEHMETOGLU, S.L. VOIT, D. HAAS, A. FERNANDEZ and Y. ARAI, "**Update on the FUTURIX-FTA Experiment in Phénix",** Proc. of GLOBAL 2005, Tsukuba, Japan, Oct 9-13, 2005 (Paper No. 448)

5. J.M. HARP, L. CAPRIOTTI, H.J.M. CHICHESTER, "**Postirradiation Examination of FUTURIX-FTA metallic alloy experiments**", J. Nucl. Mater. 515 (2019) 420–433

6. S.L. HAYES, M. K. MEYER AND D. C. CRAWFORD, G. C. CHANG and F. W. INGRAM "**Irradiation Testing of Actinide Transmutation Fuels in the Advanced Test Reactor**,**"** AppAcc-2001, Proc. Accelerator Applications/Accelerator Driven Transmutation Technology and Applications '01, Reno, NV, November 12-15, 2001, American Nuclear Society (2001).

7. P. MEDVEDEV, S. L. HAYES, S. BAYS, S. NOVASCONE, L. CAPRIOTTI, "**Testing fast reactor fuels in a thermal reactor**", Nuc. Eng. Des. 328 (2018) 154–160

8. G. S. CHANG and R. G. AMBROSEK, "**Hardening Neutron Spectrum for Advanced Actinide Transmutation Experiments in the ATR**," Radiation Protection Dosimetry (2005), Vol. 115, No. 1–4, pp. 63–68

9. J. HERCZEG and R. B. MATTHEWS, "**Advanced Accelerator Applications Program**," Proc. Accelerator Applications/Accelerator Driven Transmutation Technology and Applications '01, Reno, NV, November 12-15, 2001, American Nuclear Society (2001).

10. L. LEIBOWITZ, E. VELECKIS, R.A. BLOMQUIST, A.D. PELTON, "**Solidus and liquidus temperatures in the uranium-plutonium-zirconium system**", J. Nucl. Mater., 154 (1988) 145–153.

11. B.A. HILTON, D. L. PORTER AND S. L. HAYES **"AFC-1 Transmutation Fuels Post-Irradiation Hot Cell Examination 4 to 8 at.% Final Report**: **Irradiation Experiments AFC-1B, AFC-1F and AFC-1Æ**", INL/EXT-05-00785, rev.1, 2006.

12. J. M. HARP, L. CAPRIOTTI, H. J.M. CHICHESTER, P. G. MEDVEDEV, D. L. PORTER, S. L. HAYES, "**Postirradiation examination on metallic fuel in the AFC-2 irradiation test series**", J. Nucl. Mater. 509 (2018) 454–464

13. D. E. JANNEY, "**Metallic Fuels Handbook, Part 1: Alloys Based on U-Zr, Pu-Zr, U-Pu, or U-Pu-Zr, Including Those with Minor Actinides (Np, Am, Cm), Rare-earth Elements (La, Ce, Pr, Nd, Gd), and Y",** INL/EXT-15-36520, Revision 2 Part 1, 2017

14. D. D. KEISER., 2009. "**The development of FCCI zones in irradiated U-Zr and U-Pu-Zr fuel elements with stainless steel cladding**", in: Aasen, A., Olsson, P. (Eds.), Nuclear Reactors, Nuclear Fusion and Fusion Engineering. Nova Science Publishers, Inc., Hauppauge, NY. ISBN: 978-1606925089

15. J. M. HARP, D. L. PORTER, B. D. MILLER, T. L. TROWBRIDGE and W. J. CARMACK, "**Scanning Electron Microscopy Examination of a Fast Flux Test Facility Irradiated U-10Zr Fuel Cross-section**", J. Nucl. Mater. 494 (2017) 227–239.

16. R.G. PAHL, D.L. PORTER, D.C. CRAWFORD, L.C. WALTERS, "**Irradiation behavior of metallic fast reactor fuels**", J. Nucl. Mater. 188 (1992) 3–9.